Journal of Alloys and Compounds 739 (2018) 457–467

Contents lists available at ScienceDirect

Journal of Alloys and Compounds

journal homepage: http://www.elsevier.com/locate/jalcom

Large electric field-induced strain and large improvement in energy density of bismuth sodium potassium titanate-based piezoelectric ceramics

Supalak Manotham [a, b], Pichitchai Butnoi [a, b], Pharatree Jaita [a, c], Nitish Kumar [d, e], Komsanti Chokethawai [a], Gobwute Rujijanagul [a, f, *], David P. Cann [d]

[a] Department of Physics and Materials Science, Faculty of Science, Chiang Mai University, Chiang Mai 50200, Thailand
[b] Graduate School, Chiang Mai University, Chiang Mai 50200, Thailand
[c] Science and Technology Research Institute, Chiang Mai University, Chiang Mai 50200, Thailand
[d] Materials Science, School of Mechanical, Industrial and Manufacturing Engineering, Oregon State University, Corvallis, OR 97331, USA
[e] School of Materials Science and Engineering, The University of New South Wales, New South Wales 2052, Australia
[f] Materials Science Research Center, Faculty of Science, Chiang Mai University, Chiang Mai 50200, Thailand

ARTICLE INFO

Article history:
Received 22 June 2017
Received in revised form
15 December 2017
Accepted 16 December 2017
Available online 20 December 2017

Keywords:
Sintering
Electrical properties
Piezoelectric properties
Ferroelectric properties

ABSTRACT

Ceramic solid solutions based on (1-*x*)$Bi_{0.5}(Na_{0.84}K_{0.16})_{0.5}TiO_3$-*x*$Ba(Nb_{0.01}Ti_{0.99})O_3$ or (1-*x*)BNKT-*x*BNbT) (where $x = 0$, 0.01, 0.03, 0.05 and 0.07 mol fraction) were investigated to demonstrate the improvement of electrical properties as compared to the unmodified BNKT ceramic. The dielectric, ferroelectric, piezoelectric and electric field-induced strain properties were investigated as a function of composition and temperature. All ceramics presented a single phase perovskite structure. X-ray diffraction analysis revealed a transition from co-existing rhombohedral-tetragonal phases to a single tetragonal phase for compositions with $x > 0.03$. The maximum dielectric constant tended to increase with increasing BNbT content and the dielectric spectra for all compositions exhibited a broad maximum around T_d and T_m. The polarization hysteresis measurement indicated a disruption in the long range ferroelectric order at the critical composition of $x = 0.03$ along with a significant enhancement in the electric field-induced strains ($S_{max} = 0.41\%$) with a large normalized strain coefficient ($d^*_{33} = S_{max}/E_{max}$) of 683 pm/V. The $x = 0.03$ composition also presented a high energy density (0.67 J/cm^3) as compared with the unmodified BNKT composition (0.25 J/cm^3). These results suggest that the (1-*x*)BNKT-*x*BNbT solid solution is a promising lead-free piezoelectric material candidate.

1. Introduction

Although lead-based piezoelectric ceramics such as $Pb(Zr_xTi_{1-x})O_3$ (PZT) have excellent piezoelectric and/or electrostrictive properties [1–3], the lead constituent in these ceramics can be volatilized easily during processing and cause environmental problems. Furthermore, due to the restrictions on environmental pollution such as the waste electrical and electronic equipment (WEEE) and restriction of hazardous substance (RoHS) acts, there is a strong motivation for the development of lead-free piezoelectric ceramics capable of replacing lead-based ceramics. Recently, many reports have concentrated on the development of lead-free piezoelectric materials including compounds such as bismuth sodium titanate or $Bi_{0.5}Na_{0.5}TiO_3$ (BNT) and their solid solutions with $BaTiO_3$ (BT), $(Bi_{0.5}K_{0.5})TiO_3$ (BKT), and $K_{0.5}Na_{0.5}NbO_3$ (KNN) [4,5]. Although these materials exhibit useful electrical properties, their piezoelectric properties are generally inferior to Pb-based materials.

The BNT ceramics are A-site complex perovskites of the form A'A''BO_3, where Bi^{3+} and Na^+ ions reside on A-site, while Ti^{4+} ion occupies B-site of the perovskite unit cell [6]. At room temperature (RT), BNT has a rhombohedral perovskite symmetry with a lattice parameter of $a = 3.98$ Å and $\alpha = 89.67°$ [7]. A transformation to tetragonal symmetry occurs at temperatures around 200–340 °C, followed by a transition to cubic symmetry above 540 °C [7,8]. This material has been the subject of many studies due to its large P_r

* Corresponding author. Department of Physics and Materials Science, Faculty of Science, Chiang Mai University, Chiang Mai 50200, Thailand.
E-mail address: rujijanagul@yahoo.com (G. Rujijanagul).

https://doi.org/10.1016/j.jallcom.2017.12.175
0925-8388/

(38 μC/cm^2) and high T_c (320 °C) [8–10]. However, BNT ceramics possess inferior piezoelectric properties and present difficulties with poling because of their high conductivity and high E_c (73 kV/cm) [8,11]. Hence, the piezoelectric properties of pure BNT ceramics are significantly lower than those of the lead-based ferroelectrics, such as PZT. Most of the recent published reports on BNT ceramics have focused on improving the properties of BNT through the addition of additives to replace either or both of A or B-site ions. Moreover, there have been many reports on lead-free piezoelectric materials based on BNT solid solutions. To achieve improved piezoelectric properties, binary and ternary solid solutions based on BNT have been developed and shown to possess excellent electrical performance near the morphotropic phase boundary (MPB) composition.

Among them, the (1-*x*)BNT-*x*BKT or BNKT system presents relatively high piezoelectric and dielectric properties near the rhombohedral-tetragonal region when *x* is between 0.16 and 0.20 (*i.e.* the MPB region) [12]. This MPB region showed relatively high d_{33} of 157 pC/N and d_{31} of 46.9 pC/N [12,13]. A relatively high electric field-induced strain of 0.19% with a corresponding normalized strain coefficient ($d^*_{33} = S_{max}/E_{max}$) of ~240 pm/V was also observed. The dielectric and piezoelectric properties of BNKT ceramic were also enhanced in the MPB region, similar to that observed for Pb(Zr, Ti)O_3 ceramics [1]. In order to further improve the piezoelectric properties of the BNKT ceramic, incorporation of various dopants and the formation of solid solutions with other compounds such as $BiFeO_3$ [10], $SrTiO_3$ [14], $Bi(Mg_{0.5}Ti_{0.5})O_3$ [15], $K_{0.5}Na_{0.5}NbO_3$ [16] and $Ba_{0.5}Sr_{0.5}TiO_3$ [17] have been extensively carried out.

Many previous works have reported that Nb_2O_5 is an important additive (dopant) for improving the properties of $BaTiO_3$-based ceramics [18–21]. In some cases, this dopant can also enhance the sintering and the densification process [19,21]. Yang et al. [19] reported that Zn and Nb co-doping was effective at inhibiting grain growth, resulting in an improvement in the densification and a decrease in the dielectric loss of $BaTiO_3$-based ceramics. Osoro et al. [18] studied cobalt/niobium co-doping in $BaTiO_3$ ceramics and the piezoelectric properties of these ceramics were found to improve. Kim et al. [21] investigated the properties of $BaTiO_3$ co-doped with Nb_2O_5 and Ta_2O_5. The correlation between the sintering temperature and dielectric properties in the Nb^{5+} and Ta^{5+} doped $BaTiO_3$ solid solutions were investigated. It was found that all doped $BaTiO_3$ samples investigated had a tetragonal phase in the *P*4*mm* space group. The sample sintered 1250 °C showed smaller grain sizes (<1.0 μm) where as large grain sizes (1.5 ~ 3 μm) were observed for the samples sintered at 1300 °C. A slight shift in T_c to a lower temperature than that for pure $BaTiO_3$ was observed in all samples. A doping level of $Ba(Nb_{0.01}Ti_{0.99})O_3$ showed improvement of the dielectric constant and dielectric loss ($tan\ \delta$) values at RT. The highest value of dielectric constants at RT were >4000 and the large change of permittivity as a function of frequency were observed for the $Ba(Nb_{0.01}Ti_{0.99})O_3$ composition. At temperatures above T_c, the dielectric constant followed the Curie-Weiss law.

Recently, Cui et al. [22] synthesized $BaTiO_3$ doped with Nb via a sol-gel process. The doping shifted T_c to low temperatures and a high dielectric constant was observed for some conditions. Furthermore, it has been proposed that Nb doping can improve the piezoelectric properties of many Bi-based piezoelectric ceramics. For example, Pham et al. [1] found that Nb doping could induce a transformation from a ferroelectric to a non-polar pseudocubic phase in $Bi_{0.5}(Na_{0.82}K_{0.18})_{0.5}$ ceramics, resulting in an enhanced electric field-induced strain. The Nb substitution significantly disrupts the ferroelectric order of the $Bi_{0.5}(Na_{0.82}K_{0.18})_{0.5}TiO_3$ phase, leading to a decrease of the P_r, E_c, and d_{33} values. However, the destabilization of the ferroelectric order was accompanied by a significant enhancement in the electric-field-induced strain (EFIS) of ~0.47% ($d^*_{33} = 641$ pm/V) at the composition of $x = 0.03$ (@ 70 kV/cm). In addition, Nb-doped $(Bi_{0.5}Na_{0.4}K_{0.1})TiO_3$ lead-free piezoelectric ceramics were investigated by Wang et al. [4]. A giant strain of 0.34% was achieved at 2 mol% Nb-doping concentration with d^*_{33} of 625 pm/V. Ullah et al. [17] also found that the addition of Nb to BNKT-BSrT ceramics caused an improvement in the electric-field-induced strain. A high d^*_{33} of 634 pm/V and S_{max} of 0.38% were obtained with a 2 mol% Nb dopant under an applied field of 60 kV/cm. This indicates that an appropriate Nb-dopant content can significantly enhance the strain level of $(Bi_{0.5}Na_{0.4}K_{0.1})TiO_3$ ceramics, making it a promising candidate for actuator applications.

It has been reported that excellent piezoelectric properties are often observed in materials which are characterized by phase coexistence such as rhombohedral-tetragonal mixed phases. Furthermore, chemical modifiers are often used to disrupt the long-range ferroelectric order and promote the ergodic relaxor state of BNKT ceramics. The combination of a ferroelectric phase and a relaxor phase (after compositional modifications) can help to form an ergodic relaxor with reduced negative strains, and also result in a large electric field-induced strain [14,16].

Therefore, in the present work, the composition $Bi_{0.5}(Na_{0.84}K_{0.16})_{0.5}TiO_3$ or BNKT which is at the MPB composition (within the rhombohedral-rich phase) was selected as the base material. $BaTiO_3$ doped with Nb with the composition of $Ba(Nb_{0.01}Ti_{0.99})O_3$, BNbT (tetragonal-rich phase) [21]. was chosen as part of the solid solution with BNKT. To our knowledge, the effects of BNbT on the properties of BNKT ceramics have not yet been investigated. It is expected that this new system has great potential for excellent electrical performance as compared to the BNKT system or other systems.

2. Experimental

2.1. Synthesis

$Bi_{0.5}(Na_{0.84}K_{0.16})_{0.5}TiO_3$ or BNKT and $Ba(Nb_{0.01}Ti_{0.99})O_3$ or BNbT powders were separately prepared by a conventional solid-state reaction method. The analytical grade reagents of Bi_2O_3 (98%, Sigma-Aldrich), Na_2CO_3 (99.5%, Sigma-Aldrich), TiO_2 (99%, Sigma-Aldrich), K_2CO_3 (99%, Sigma-Aldrich), $BaCO_3$ (98.9%, Sigma-Aldrich) and Nb_2O_5 (99.9%, Sigma-Aldrich) were used as starting materials. The raw materials of BNKT and BNbT were stoichiometrically weighed, ball milled for 24 h in an ethanol solution, and dried in an oven. Due to a large difference in calcination temperatures between $Bi_{0.5}(Na_{0.84}K_{0.16})_{0.5}TiO_3$ (900 °C) and $Ba(Nb_{0.01}Ti_{0.99})O_3$ (1300 °C) powders, the $Bi_{0.5}(Na_{0.84}K_{0.16})_{0.5}TiO_3$ and $Ba(Nb_{0.01}Ti_{0.99})O_3$ powders were therefore synthesized separately. The BNKT and BNbT powders were calcined at 900 °C and 1300 °C, respectively. The obtained powders were then weighed, mixed and dried again to produce powder of (1-*x*)$Bi_{0.5}(Na_{0.84}K_{0.16})_{0.5}TiO_3$-*x*$Ba(Nb_{0.01}Ti_{0.99})O_3$ or (1-*x*)BNKT-*x*BNbT ($x = 0$, 0.01, 0.03, 0.05 and 0.07 mol fraction). A few drops of 4 wt% polyvinyl alcohol (PVA) binders were then added to the mixed powders before being uniaxially pressed into 10 mm diameter discs. These pellets were covered with sacrificial powders and then sintered at 1125 °C for 2 h with a heating/cooling rate of 5 °C/min.

2.2. Characterization

An X-ray diffractometer (XRD-Phillip, X-pert) was used to identify the phases present in both powders and ceramics. Raman spectra were obtained on polished sintered pellets with a Raman spectrometer (T6400 JY, Horiba Jobin Yvon). Bulk density was

measured in accordance with Archimedes' method. A scanning electron microscope (SEM, JEOL JSM- 6335F) was used to study microstructural features of the ceramics. Grain size was determined by a mean linear intercept method (ASTM E112-88). Before being subjected to electrical characterization, all samples were carefully polished to 1 mm thickness to obtain a parallel scratch-free surface. Silver paste was painted onto both sides of each sample and then fired at 700 °C for 30 min to form electrodes. Dielectric properties as a function of temperature (25–500 °C) were carried out using a 4192A LCR-meter connected to a high temperature furnace with frequencies ranging from 1 to 500 kHz. A ferroelectric system based on Radiant Precision High Voltage Interface was used to measure the polarization-electric field (*P-E*) hysteresis loops both at RT and high temperatures (25–150 °C). A maximum electric field of 60 kV/cm and a frequency of 1 Hz were applied to each sample. Remanent polarization (P_r), maximum polarization (P_{max}), coercive field (E_c), and loop squareness (R_{sq}) values were determined from the hysteresis loops. Strain-electric field (*S-E*) data at RT was obtained using an optical displacement sensor (Fotonic Sensor, MTI-2100) combined with a Radiant ferroelectric test system. A maximum electric field of 60 kV/cm and a frequency of 0.1 Hz were applied for each sample to measure the butterfly curves. The maximum strain (S_{max}), the negative strain (S_{neg} denotes the difference between zero-field strain and the lowest strain and is only visible in the bipolar cycle) were carried out. The high field longitudinal piezoelectric constant or the normalized strain coefficient (d^*_{33}) was determined from the ratio of maximum strain to maximum field using an empirical equation (1) [16,17]:

$$d^*_{33} = S_{max}/E_{max} \quad (1)$$

3. Results and discussion

The mixed powders of the (1-*x*)BNKT-*x*BNbT were characterized using XRD analysis over a wide 2θ range of 20–80° as shown in Fig. 1(a). The unmodified BNKT powder exhibited a single perovskite structure and also exhibited rhombohedral symmetry. After the addition of BNbT, the XRD patterns displayed a phase mixture between BNKT and BNbT. The intensity of the BNbT peaks increased with BNbT content. Furthermore, there were no secondary peaks for all modified powders within the detection limits of the XRD instrument.

The X-ray diffraction patterns obtained from each of the (1-*x*) BNKT-*x*BNbT ceramic samples within a 2θ range of 20–80° are shown in Fig. 1(b). All (1-*x*)BNKT-*x*BNbT ceramics exhibited a single perovskite structure with no trace of secondary phases which suggests that a complete solid solution was formed. The position of all XRD peaks for the modified samples shifted slightly to lower 2θ angles in comparison with the unmodified BNKT ceramic. This observation implies a change in the *d*-spacing as a result in change of lattice parameters for the BNKT phase, as seen in Fig. 2. In this work, it is expected that Ba^{2+} ($r^{2+}_{Ba} = 1.42$ Å) substituted onto the A-site [K^+ ($r^{+}_{K} = 1.33$ Å), Na^+($r^{+}_{Na} = 1.18$ Å) and Bi^{3+} ($r^{3+}_{Bi} = 1.17$ Å)], while Nb^{5+} ($r^{5+}_{Nb} = 0.64$ Å) [17] substituted onto the B-site [Ti^{4+} ($r^{4+}_{Ti} = 0.74$ Å)] [23] to form the (1-*x*)BNKT-*x*BNbT solid solution [24].

A detailed view of the XRD patterns at 2θ ~39–41° and 45–47° are shown in Fig. 1(c) and (d), respectively. The XRD data revealed that the unmodified BNKT ceramic had a rhombohedral symmetry as evidenced by the splitting of $(111)_R/(1\bar{1}1)_R$ peaks. In addition, it was evident that the $x = 0.03$ composition exhibited a phase mixture of rhombohedral and tetragonal phases due to splitting of

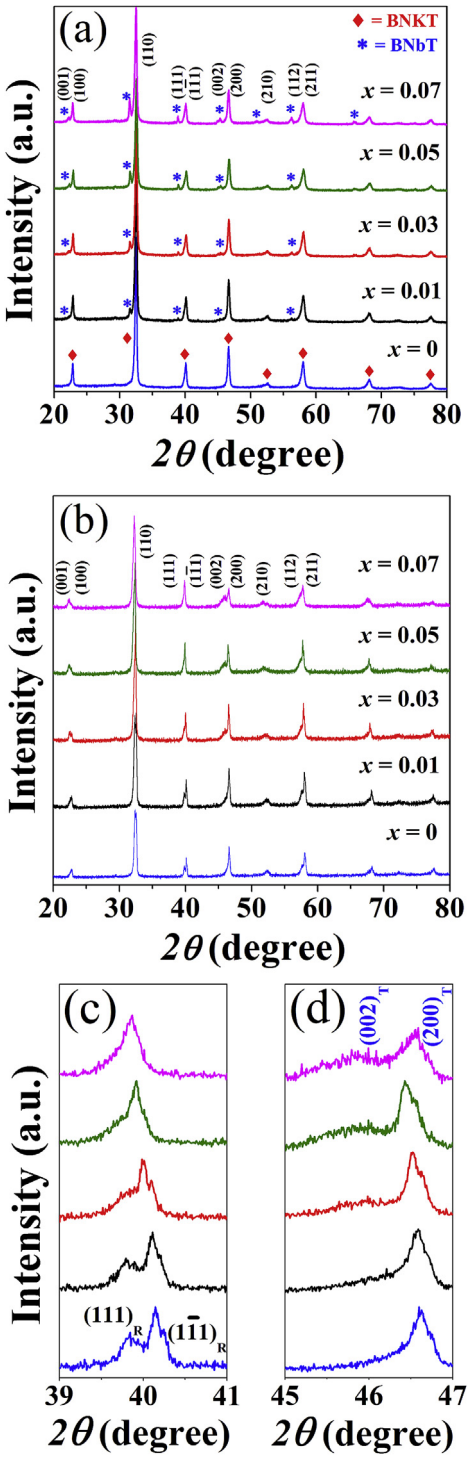

Fig. 1. X-ray diffraction of the (1-*x*)BNKT-*x*BNbT including (a) mixed calcined powder (b) sintered ceramics, and (c,d) corresponding detailed view of the XRD patterns.

the $(111)_R/(1\bar{1}1)_R$ peaks at 2θ ~ 40° and a slight splitting of the $(200)_T/(002)_T$ peaks at 2θ ~ 46° [1,24–27]. With increased amount of BNbT ($x > 0.03$), the crystal structure tended to change with the observation of the $(111)_R/(1\bar{1}1)_R$ peaks which were split the rhombohedral peaks for the unmodified BNKT ceramics and then merged into a single $(111)_T$ peak along with more apparent splitting of the tetragonal $(200)_T/(002)_T$ peaks for the modified samples. This clearly indicates a transformation from mixed rhombohedral/

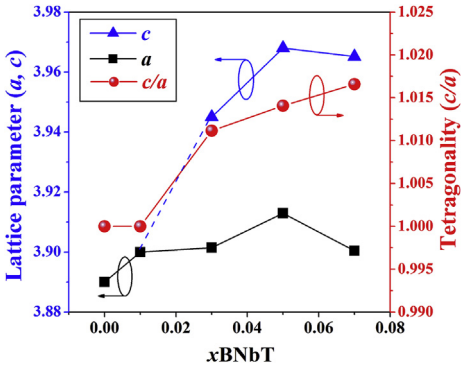

Fig. 2. Plots of lattice constants (*a* and *c*) and the tetragonality (*c*/*a*) as functions of BNbT content for the (1-*x*)BNKT-*x*BNbT ceramics.

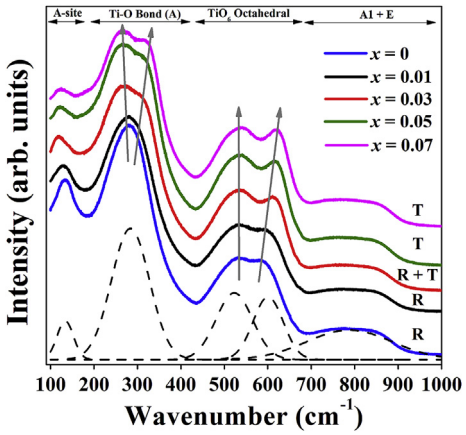

Fig. 3. Raman spectra of the (1-*x*)BNKT-*x*BNbT ceramics at room temperature. The dash line was accorded to five Gaussian-Lorentzian mode fitting.

tetragonal phase for the $x = 0.03$ compositions into a tetragonal phase for the compositions with $x > 0.03$. Similar results have been reported in BNKT-based systems such as BTS-modified BNKT [24], CuO and Nb_2O_5 co-doping BNKT [26], and LMN-doped BNKT-ST system [27]. Therefore, the phase coexistence for the present ceramics occurred at $x = 0.03$. To confirm the appearance of the phase transformation in more detail, the *a* and *c*-parameters and tetragonality ratio (*c*/*a*) were determined, using the following expression [28]:

$$\frac{1}{d^2} = \frac{h^2 + k^2}{a^2} + \frac{l^2}{c^2} \quad (2)$$

where *d* is a plane spacing, *a* and *c* are lattice parameters, and *h, k, l* are Miller indices. From the calculation, an increase in *c*/*a* value was observed as the BNbT content increased as expected (see Fig. 2 and Table 1).

To further confirm the phase structure of the studied samples, Raman spectroscopy was used. The Raman spectra (from 100 to 1000 cm^{-1}) of ceramics at RT are shown in Fig. 3. According to previous reports [29–31], it is clearly seen that the normal mode vibrations are responsible for the Raman lines. First, a Raman-active mode observed between 100 and 200 cm^{-1} is related to the vibration of A-site cations in the perovskite structure, which could be due to cation distortions or clusters of octahedra [BiO_6] and [NaO_6] [29]. It is interesting to note that the addition of BNbT tended to show a slight decrease in the intensity of A-site peak of (1-*x*)BNKT-*x*BNbT. This suggests that the BNbT additive may induce cationic disorder in the lattices. The peak at centered ~280 cm^{-1} is associated with the Ti-O vibrations [30]. Moreover, with increased BNbT concentrations, the peak split into two bands at ~264 and ~321 cm^{-1}. This correlates well with the XRD analysis which indicates that the crystal structure of (1-*x*)BNKT-*x*BNbT ceramics transformed from rhombohedral (*R3c*) symmetry (for $x < 0.03$) into a coexistence of rhombohedral and tetragonal (*P4bm*) (for $x = 0.03$) phases, and then finally into a tetragonal phase (for $x > 0.03$). Similar observations have been reported in other BNT-based materials [2,29]. The peak range ~450–650 cm^{-1} can be associated with the vibration of the TiO_6 octahedral [30,31]. It can be seen that the peaks shifted slightly, suggesting a distortion in the TiO_6 octahedral and a presence of internal stresses that could possibly stabilize the room temperature dielectric and ferroelectric properties with BNbT addition [31].

The selected SEM micrographs of as-sintered surfaces and grain size distribution of (1-*x*)BNKT-*x*BNbT ceramics ($x = 0$, 0.03 and 0.07) are shown in Fig. 4. From the SEM images, the samples were dense with a well-developed microstructure and a granular morphology. All ceramics showed a clear cubic-like shape and a monomodal grain size distribution. Plots of the average grain size and density values as a function of BNbT content are shown in Fig. 5. According to the linear intercept method, the average grain size of the unmodified BNKT was found to be 1.14 μm with a wide distribution when compared to some modified samples. The addition of BNbT to the BNKT ceramic, however, slightly inhibited grain growth behavior and showed a more narrow grain size distribution. This can be seen from the slight drop in the grain size value from 1.14 μm for the unmodified BNKT to around 0.60 μm for the $x = 0.07$ sample. It is believed that the observed grain morphology and slight reduction in grain size with a narrow grain size distribution for the modified sample was due to the solute drag effect of the addition of Nb^{5+}. Solute diffusion near the grain boundary region is usually slower than intrinsic diffusion of the host atoms across the boundary plane and this becomes rate-limiting for grain boundary movement [32]. This seems to be the main mechanism governing the observed microstructure, similar to those reported in a number of previous works on solid solutions and doped systems, especially for Nb-additions to $BaTiO_3$ [19]. The density value of the (1-*x*)BNKT-*x*BNbT ceramics is also presented in Table 1 and Fig. 5. It was found that all ceramics were dense with density values in the range of 5.84–5.88 g/cm^3.

The temperature dependence of the dielectric constant (ε_r) and dielectric loss (*tan δ*) for the (1-*x*)BNKT-*x*BNbT ceramics measured

Table 1
Physical, phase, microstructure and dielectric properties of (1-*x*)BNKT-*x*BNbT ceramics.

x	Density (g/cm^3)	*c*/*a*	Grain size (μm)	T_d (°C)	T_m (°C)	$\varepsilon_{r,RT}$ (1 kHz)	$\varepsilon_{r,max}$ (1 kHz)	ΔT_m (K)	γ	δ_γ (K)
0	5.88	1.000	1.14	164	301	966	4930	5.7	1.56	411
0.01	5.86	1.000	1.08	140	305	1245	5050	7.3	1.91	409
0.03	5.86	1.011	0.89	125	306	1815	5350	7.7	1.95	404
0.05	5.84	1.014	0.67	129	306	1579	5460	8.0	1.96	404
0.07	5.84	1.016	0.60	127	307	1568	5470	7.8	1.96	403

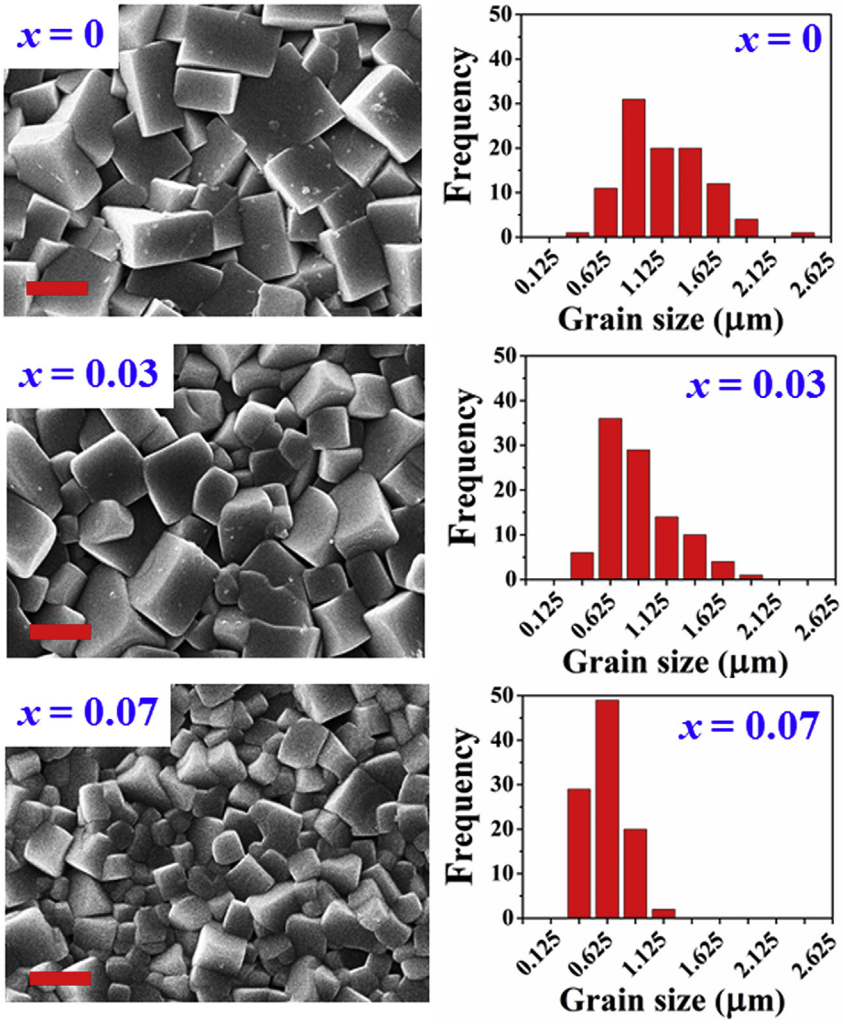

Fig. 4. Selected SEM micrographs and grain size distribution of the (1-*x*)BNKT-*x*BNbT ceramics where $x = 0$, 0.03 and 0.07 (bar = 1 μm).

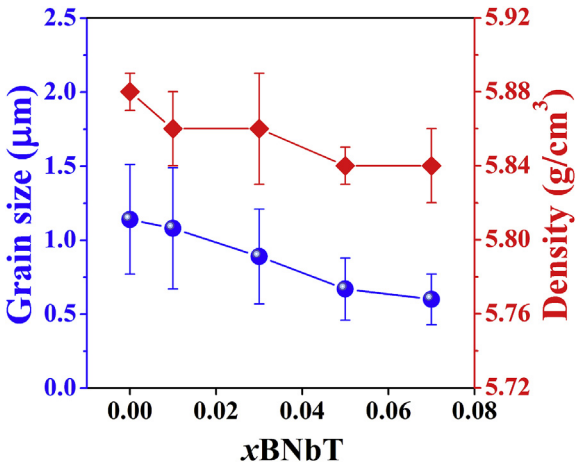

Fig. 5. Plots of grain size and density values as functions of BNbT content.

at various frequencies from 1 kHz to 500 kHz are shown in Fig. 6. A summary of the dielectric properties are also presented in Table 1. All samples showed broad peaks with a frequency dispersion of ε_r and *tan δ* near $T \sim T_m$. This behavior agrees well with the dielectric behavior of other BNT-based and BNKT-based ceramics [33–36]. Two dielectric anomalies were observed in the dielectric curves of the (1-*x*)BNKT-*x*BNbT ceramics. The first dielectric anomaly below 200 °C is often designated as the depolarization temperature (T_d), where the ferroelectricity significantly decreases. The second anomaly (~300 °C) at which the dielectric constant reaches its maximum value is called T_m [37]. Normally, there are many methods to determine T_d value (as can be found in the literature) [38]. In this work, however, the shoulder of the dielectric peak, corresponding to the inflection point in the dielectric loss curve, was used to determine the T_d value. The dielectric constant at T_m ($\varepsilon_{r,max}$) tended to increase with BNbT content (inset of Fig. 7). Furthermore, the dielectric curves of all ceramics exhibited broad transition peaks around T_d and T_m, which showed the characteristics of a diffuse phase transition [37,39]. This could be attributed to the compositional fluctuations occurring on the A and/or B sites [37]. The unmodified BNKT ceramic exhibited a T_d peak at ~164 °C. T_d tended to shift to a lower temperature with increasing BNbT content (Fig. 7).

To evaluate the evolution of relaxor behavior in the (1-*x*)BNKT-*x*BNbT ceramics, several empirical laws were employed. The simplest one is the temperature span (ΔT_m) of dielectric peaks between the lowest and highest frequencies, as the following equation [40,41]:

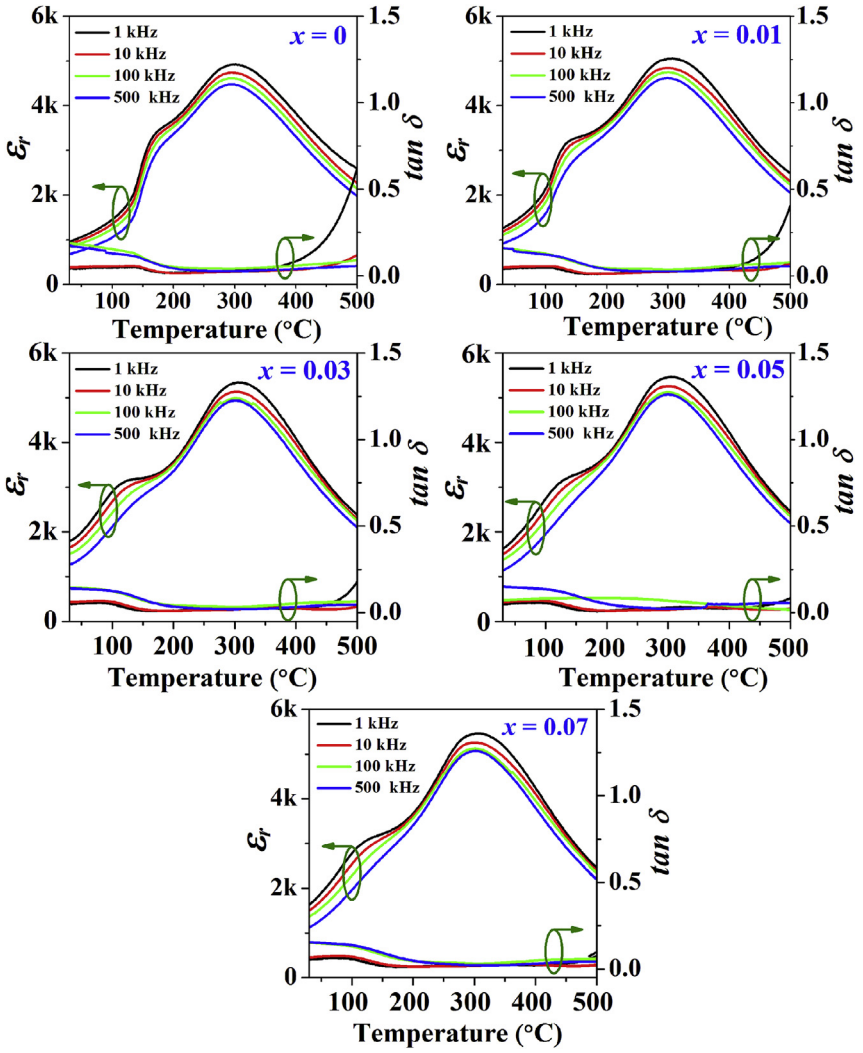

Fig. 6. Temperature dependence of dielectric constant (ε_r) and dielectric loss ($tan\ \delta$) of the (1-x)BNKT-xBNbT ceramics, measurement at various frequencies where x = 0–0.07.

$$\Delta T_m = T_m\,(@500\ \text{kHz}) - T_m\,(@1\ \text{kHz}) \tag{3}$$

where T_m is the temperature of the maximum dielectric constant. The value of ΔT_m was 5.7 K for unmodified BNKT ceramic, and it increased to ~7.8–8.0 K for the x = 0.05–0.07 compositions.

Normally, for relaxor ferroelectric materials, the dielectric behavior with a diffuse phase transition has been well described by the modified Curie-Weiss law, which is given by Refs. [42,43].

$$\frac{\varepsilon_{max}}{\varepsilon_r} = 1 + \frac{(T - T_m)^{\gamma}}{2\delta_{\gamma}^2} \tag{4}$$

where T is the absolute temperature, T_m is the temperature of the maximum dielectric constant, ε_r is dielectric constant, ε_m is the maximum dielectric constant at T_m. The parameter γ gives the information on the character of the phase transition. The value of γ is the expression of the degree of dielectric relaxation in the relaxor ferroelectric material. For γ = 1, a normal ferroelectric [44] corresponding to the Curie-Weiss law is obtained, while γ = 2 corresponds to relaxor behavior [45]. Many relaxor ferroelectric materials can be fitted by Eq. (4) with γ = 2 at temperatures above T_m. The values of γ for the (1-x)BNKT-xBNbT ceramics at 10 kHz were obtained from the slope of ln ($\varepsilon_{max}/\varepsilon_r$ - 1) vs ln (T - T_m) according to Eq. (4) and the unmodified sample had γ = 1.56 while the γ values were around 1.91–1.96 for modified samples, as listed in Table 1. This indicates that the relaxor behavior is stronger for the

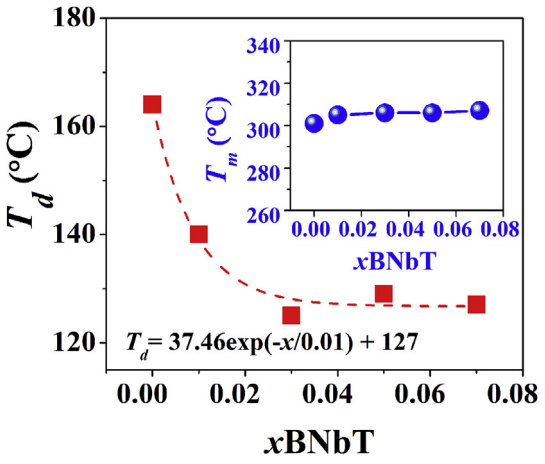

Fig. 7. A plot of T_d value as a function of BNbT content (inset: T_m value as a function of BNbT content).

compositions with a higher BNbT concentration. Furthermore, the parameter δ_γ can be used to measure the degree of diffuseness of the phase transition in mixed relaxor-normal ferroelectric materials [45]. However, the δ_γ value decreased with increasing the amount of BNbT. This may be due to the compositional change and grain characteristic (microstructure modification) as proposed in previous work [37].

The polarization-electric field (*P-E*) hysteresis data for (1-*x*) BNKT-*x*BNbT ceramics are shown in Fig. 8. The compositional dependence of P_r and E_c values are plotted in Fig. 9. To verify the quantification of changes in the hysteresis data, the loop squareness (R_{sq}) was calculated from equation (5):

$$R_{sq} = (P_r/P_s) + (P_{1.1E_c}/P_r) \quad (5)$$

where P_r is remanent polarization, P_s is saturated polarization and E_c is coercive field [46]. The remanent polarization (P_r), coercive field (E_c) and loop squareness (R_{sq}) are also listed in Table 2. All samples exhibited ferroelectric behavior at RT. The unmodified BNKT ceramic displayed a typical ferroelectric *P-E* loop with a maximum coercive field (E_c = 42.4 kV/cm), remanent polarization (P_r = 29.3 μC/cm^2), and loop squareness (R_{sq} = 1.25). The obtained trends in ferroelectric properties are in good agreement with similar compositions as reported by Zheng et al. [47]. In the present work, current versus applied electric field plots (*I-E* loops) were also carried out (Fig. 8). Normally, a sharp polarization current peak

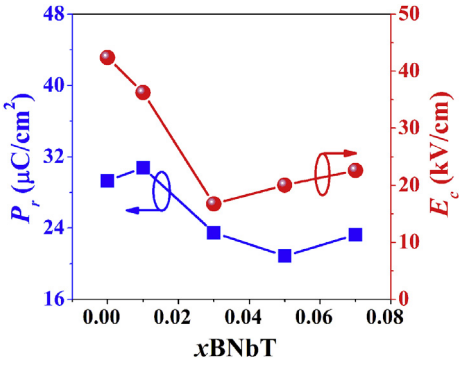

Fig. 9. Plots of P_r and E_c values as a function of BNbT content.

(denoted as point 1 in *I-E* loop) can be ascribed to domain switching. However, the BNbT additive significantly influenced the shape and properties of the *P-E* loop. Specifically, the addition of BNbT produced a slight degradation in ferroelectric behavior, as can be noted by the change of P_r and E_c values, where the minimum values of P_r and E_c were found at the $x = 0.05$ and $x = 0.03$ ceramics, respectively. In addition, clear evidence of pinched *P-E* loops could also be observed for the $x = 0.03$ ceramic. The appearance of the pinched *P-E* loops is concurrent with two current peaks (denoted as 1 and 2) in the *I-E* data [48]. The decreasing P_r and E_c values indicate

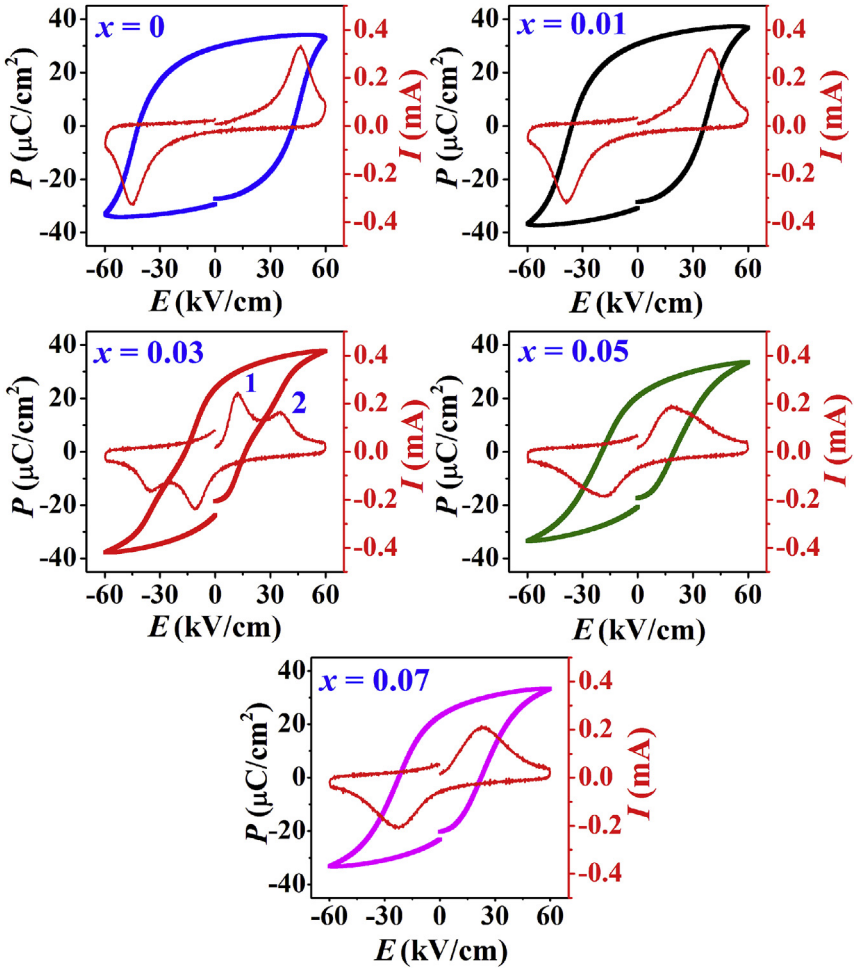

Fig. 8. Polarization-electric field (*P-E*) hysteresis loops and current-electric field (*I-E*) loops for the (1-*x*)BNKT-*x*BNbT ceramics, where $x = 0$–0.07.

Table 2
Ferroelectric and piezoelectric properties of (1-*x*)BNKT-*x*BNbT ceramics.

x	P_r (μC/cm^2)	E_c (kV/cm)	R_{sq}	J^a (J/cm^3)	η^a (%)	S_{max} (%)	S_{neg} (%)	d^*_{33} (pm/V)	Q_{33} (m^4/C^2)
0	29.3	42.4	1.25	0.25	23	0.12	0.07	200	0.007
0.01	30.3	38.3	1.14	0.60	51	0.19	0.09	317	0.015
0.03	23.5	16.7	0.74	0.67	75	0.41	0.19	683	0.030
0.05	20.9	20.0	0.77	0.58	70	0.23	0.06	383	0.022
0.07	23.2	22.6	0.87	0.51	62	0.18	0.06	300	0.016

[a] Ferroelectric data obtained at high temperature of 150 °C and a frequency of 1 Hz.

that the ferroelectric (FE) state was weakened and the ergodic relaxor (ER) phases appeared in the modified samples under zero electric field. The slightly pinched loops observed for the $x = 0.03$ ceramic suggests that the long range ferroelectric order (dominant in the unmodified BNKT ceramic) was disrupted by the addition of BNbT along with a transition from a ferroelectric (FE) to ergodic relaxor (ER) state. This ergodic relaxor state can be transformed reversibly into ferroelectric state by an external electric field, and does not maintain the long-range FE behavior when the E-field is removed [49,50].

Since the stability of the FE phase depends not only on composition but also on temperature, the temperature-dependent ferroelectric properties were investigated. Fig. 10 shows temperature dependent polarization-electric field (*P-E*) hysteresis data for (1-*x*)BNKT-*x*BNbT ceramics. The effect of temperature on the *P-E* hysteresis data was measured under a maximum electric field of 60 kV/cm and a frequency of 1 Hz. The unmodified sample exhibited well-saturated *P-E* hysteresis loops at RT. With increasing the temperature up to 125–150 °C, a slimmer loop was observed. For $x = 0.03$ sample, a slight pinching in the loops was observed at RT. With further increasing the temperature to 75 °C, the P_r and E_c values dramatically decreased and the hysteresis loops started to deform and began to show constricted loops, followed by a pinched shape at temperatures around 75 °C (as indicated by "*"). This type of behavior in the temperature dependent hysteresis loops has also been observed in other BNT-based materials [50–52]. Thus, both chemical modification and temperature change can disrupt the FE long-range order leading to a decrease in the polarization states.

Plots of energy storage density (*W*) as a function of temperature of (1-*x*)BNKT-*x*BNbT ceramics are also shown in Fig. 11. The *W* value was calculated from the *P-E* hysteresis loops in order to evaluate the practicability of these ceramics for energy storage systems. The energy storage density was calculated using the following formula (6):

$$W = \int E dP \tag{6}$$

where *E* is the applied electric field and *P* is polarization [27,53–55]. The *W* values at 150 °C are also listed in Table 2. The unmodified BNKT ceramic had an energy density of 0.09 J/cm^3 at RT (Fig. 11). The energy density increased with increasing temperature, and reached ~0.25 J/cm^3 at 150 °C. The addition of BNbT into BNKT was found to improve the energy density value. The $x = 0.03$ sample showed the highest energy density of 0.67 J/cm^3 (at 150 °C), which was higher than its value measured at RT (0.28 J/cm^3) by 139% and also higher than the value for the unmodified ceramic (measured at 150 °C) by ~ 168%. Furthermore, the obtained value also indicates a very large enhanced value as compared to the unmodified BNKT ceramic (measured at RT) by 644%. This value is comparable to the previously reported of BNKT-based bulk ceramics studied by Malik et al. [56] which showed an energy density value of ~0.65 J/cm^3 (measured at 75 °C). It has been observed that the high *W* composition often lies at the boundary between the ER and FE states. Normally, *W* also depends on the shape of *P-E* hysteresis

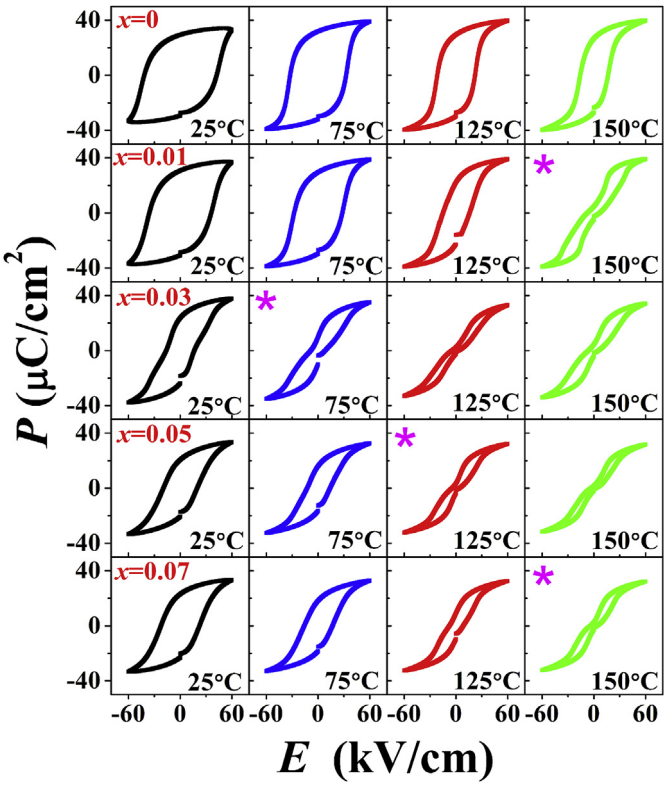

Fig. 10. Temperature dependence on polarization-electric field (*P-E*) hysteresis loops of the (1-*x*)BNKT-*x*BNbT ceramics measured under an electric field of 60 kV/cm and a frequency of 1 Hz; where "*" indicates trend of temperature at which a sample start to show a clear pinched loop.

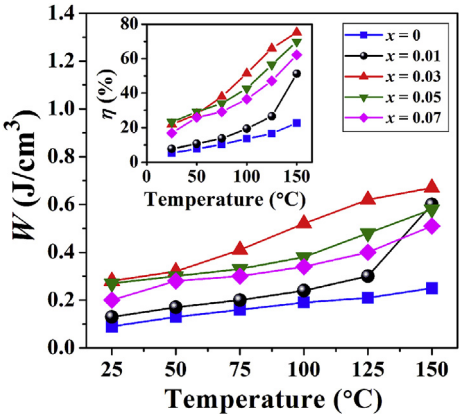

Fig. 11. Energy storage density (*W*) as a function of temperature of the (1-*x*)BNKT-*x*BNbT ceramics (Inset: energy storage efficiency (η) as a function of composition at different temperatures).

loop, *i.e.* the *P-E* hysteresis loop can transform from a square ferroelectric loop to a slim loop at temperatures approaching T_d. This can yield a high energy density. Furthermore, Zhao et al. [55] reported that the energy storage in ceramics with "slanted" and "slender" *P-E* loops intrinsically possess a higher energy storage density than that of "square" loops, which is also in good agreement with our findings. In the present work, W increased with increasing temperature and the maximum W was observed near T_d [27]. Again, similar behavior has been observed in previous reports [27,56].

For practical applications, energy storage efficiency (η) is often considered. The η value was calculated via the following formula (7):

$$\eta = \frac{W}{W + W_{loss}} \times 100 \quad (7)$$

where W_{loss} is the energy loss density [56,57]. It can also be observed that the η value was affected by BNbT content and temperature (inset of Fig. 11). In this work, the maximum η value of 75% and energy density of 0.67 J/cm^3 (at 150 °C) were observed for the $x = 0.03$ sample. The obtained results indicate that this material is considered as favorable for high temperature energy storage capacitor applications [56].

Fig. 12(a–e) illustrates the bipolar field-induced strain curves at RT of (1-x)BNKT-xBNbT ceramics for the compositions $x = 0.00$–0.07. Values of maximum strain (S_{max}) and the normalized strain coefficient ($d^*_{33} = S_{max}/E_{max}$) as a function of BNbT content are displayed in Fig. 13. The negative strain (S_{neg}), S_{max}, and

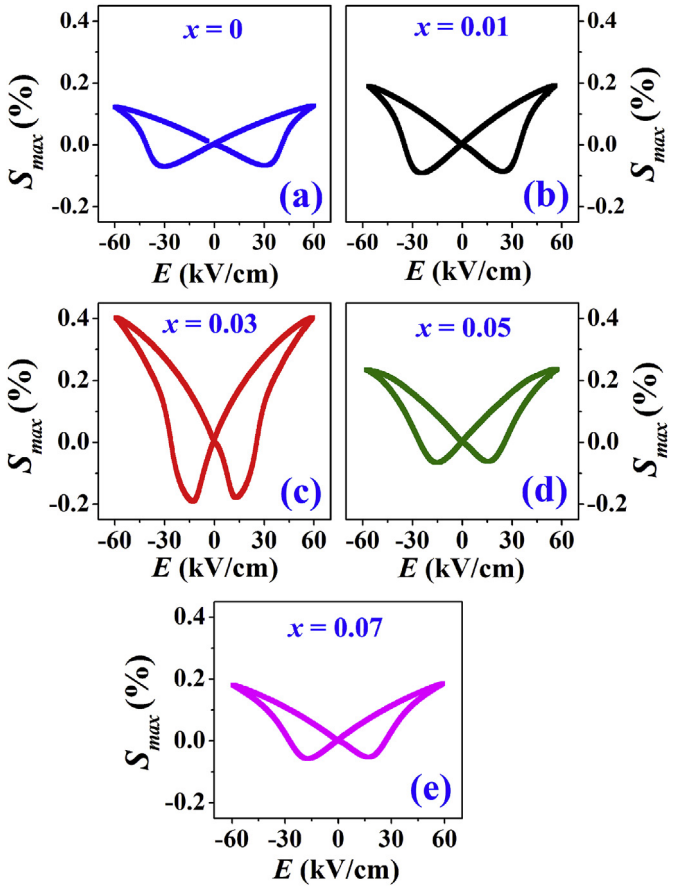

Fig. 12. Bipolar strain-electric field (*S-E*) loops of the (1-x)BNKT-xBNbT ceramics, where (a) $x = 0$, (b) $x = 0.01$, (c) $x = 0.03$, (d) $x = 0.05$, and (e) $x = 0.07$.

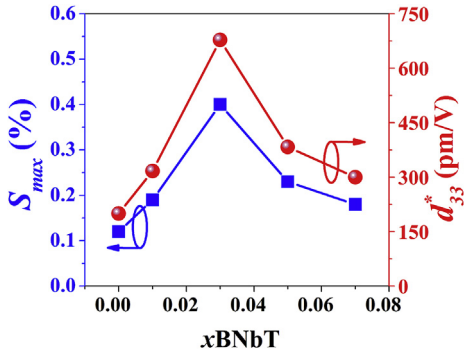

Fig. 13. Plots of the maximum strain (S_{max}) and the normalized strain coefficient ($d^*_{33} = S_{max}/E_{max}$) as a function of BNbT content.

d^*_{33} values are summarized in Table 2. The value for S_{neg} was calculated as the difference between the zero-field strain and the maximum negative strain, which can be closely related to domain switching during bipolar cycling. The unmodified BNKT ceramic exhibited a classic butterfly shaped loop with a clearly defined negative strain. This behavior is a common characteristic of normal ferroelectric (FE) materials [56,58]. In this case, this sample had values $S_{max} = 0.12\%$, $d^*_{33} = 200$ pm/V and $S_{neg} = -0.07\%$. The S_{max} and S_{neg} values clearly increased with increasing BNbT content, and S_{max} reached the maximum value of 0.41% with $d^*_{33} = 683$ pm/V and $S_{neg} = -0.19$ for the $x = 0.03$ ceramic. The obtained d^*_{33} value is ~242% higher than that of the unmodified sample. However, a further increase of BNbT content ($x > 0.03$) resulted in a decrease of S_{max} and d^*_{33} values (see Table 2). The large S_{max}, d^*_{33} and S_{neg} values for $x = 0.03$ are likely due to the electric field-induced reversible phase transition between the FE and ER states [59]. The applied electric field drives the phase transition from the ER state to the FE state because of the competitive free energy between these two phases [37,60]. This often results in an increase of the strain and significantly improves the piezoelectric properties. Similar results were reported by Zhang et al. [60], who studied the $Bi_{0.5}Na_{0.5}TiO_3$-$BaTiO_3$-$K_{0.5}Na_{0.5}NbO_3$ (BNT-BT-KNN) system. They found that BNT-BT system delivered a large strain response of 0.45% (at 8 kV) when a small amount of BNT was replaced by KNN. This giant strain was attributed to a combination of field-induced phase transition and ferroelectric domain reorientation. In the present work, it should be noted that the improvement of strain response for the $x = 0.03$ ceramic can be correlated with XRD data which indicates the coexistence of rhombohedral and tetragonal phases. Moreover, the large improvement in the strain response for the $x = 0.03$ ceramic may also be due to the decrease in the depolarization temperature (T_d) which correlates with the pinching of the *P-E* hysteresis loop. This indicates a transition from a FE state to an ER state near T_d [2]. Dong et al. [5] observed similar behavior in the (1-x)($0.8Bi_{0.5}Na_{0.5}TiO_3$-$0.2Bi_{0.5}K_{0.5}TiO_3$)- $xNaNbO_3$ system. In their work, a large S_{max}/E_{max} value of 810 pm/V was observed at a temperature of 30 °C, which was proposed to be due to the shift of T_d down to below room temperature. In general, the transition from the ferroelectric state to the relaxor state is characterized by a shift from pinched *P-E* loops to sprout-shaped *S-E* loops, depending upon the composition. In the appropriate range of composition, the free energy difference between the two phases is small enough and the application of a moderate electric field is sufficient to switch the relaxor state to the ferroelectric state resulting in a large strain [5]. Pham et al. [1] also studied Nb-substituted $Bi_{1/2}(Na_{0.82}K_{0.18})_{1/2}TiO_3$ lead-free ceramics and found that the addition of 3 mol% Nb into $Bi_{1/2}(Na_{0.82}K_{0.18})_{1/2}TiO_3$ shifted T_d value to a lower temperature (99 °C) and resulted a high strain value. Furthermore, several reports

for the chemically-modified BNT-based and BNKT-based ceramics have also noted that the phase transition (between the FE and ER states) seems to be the key to maximum electric-field-induced strain values [27,37,49,61].

To have a further understanding for the electrostriction coefficient (Q_{33}), the relationship between Q_{33}, S and P was investigated. Normally, the strain has a parabolic relationship to the polarization, as can be expressed in equation (8) [62,63].

$$S_3 = Q_{33}P_3^2 \tag{8}$$

where Q_{33} is the electrostriction coefficient, S_3 is the strain and P_3 is the polarization in the direction of the poling axis. Based on the calculated Q_{33} of (1-x)BNKT-xBNbT ceramics as shown in Table 2, it was found that the maximum Q_{33} value of 0.030 m^4/C^2 was observed for the $x = 0.03$ sample. It can be seen that the obtained Q_{33} value is relatively high as compared to those of well-know electrostrictive materials such as BNT-BT-KNN (0.021 m^4/C^2) [63], BNKT-KNN (0.023 m^4/C^2) [64], and BNKT-BZ (0.025 m^4/C^2) [65].

Based on the obtained results, the compositions near the transition from rhombohedral symmetry to the coexistence of rhombohedral and tetragonal phases ($x = 0.03$) are host to a significant enhancement in piezoelectric properties and energy density. This significant electrical enhancement at the composition of $x = 0.03$ can be related to both a composition-induced structural phase transition and a field-induced ergodic relaxor (ER to FE) phase transition. Grain size is another factor which has been proposed to affect many properties of electroceramics [3]. Further work is required to understand this effect in more detail. However, other factors such as density, phases, and defects (in the samples) should be carefully controlled by designing a proper experiment.

4. Conclusions

Lead-free piezoelectric ceramics of (1-x)BNKT-xBNbT were successfully synthesized via the solid-state reaction technique. A single phase perovskite structure was achieved for all compositions, suggesting that a solid solution between BNKT and BNbT was obtained. The composition $x = 0.03$ was characterized by the coexistence of rhombohedral and tetragonal phases. The maximum dielectric constant peak tended to increase (4900 to 5500) with increasing BNbT content. The $x = 0.03$ ceramic exhibited large S_{max}, d^*_{33} values and W values. Based on these results, compositions near the transition from rhombohedral symmetry to the coexistence of rhombohedral and tetragonal phases are host to a significant enhancement in the dielectric, ferroelectric and piezoelectric properties. This ceramic system can be considered as one of the promising candidate materials for lead-free piezoelectric applications.

Acknowledgements

This work was supported by the Thailand Research Fund (TRF, BRG6080002 and IRG5780013), National Research University (NRU) Project under Thailand's Office of the Higher Education Commission and CMU 50th anniversary Ph.D. Grant from Chiang Mai University. Department of Physics and Materials Science, Faculty of Science, the Graduate School of Chiang Mai University, Science and Technology Research Institute, Chiang Mai University, Thailand are also acknowledged.

References

[1] K.N. Pham, A. Hussain, C.W. Ahn, I.W. Kim, S.J. Jeong, J.S. Lee, Giant strain in Nb-doped $Bi_{0.5}(Na_{0.82}K_{0.18})_{0.5}TiO_3$ lead-free electromechanical ceramics, Mater. Lett. 64 (2010) 2219–2222.
[2] P.Y. Chen, C.S. Chen, C.S. Tu, T.L. Chang, Large E-field induced strain and polar evolution in lead-free Zr-doped 92.5%$(Bi_{0.5}Na_{0.5})TiO_3$-7.5%$BaTiO_3$ ceramics, J. Eur. Ceram. Soc. 34 (2014) 4223–4233.
[3] Z. Zhao, V. Buscaglia, M. Viviani, M.T. Buscaglia, L. Mitoseriu, A. Testino, M. Nygren, M. Johnsson, P. Nanni, Grain-size effects on the ferroelectric behavior of dense nanocrystalline $BaTiO_3$ ceramics, Phys. Rev. B 70 (2004), 024107.
[4] C. Wang, T. Xia, X. Lou, S. Tian, Giant strain response in 2 mol% Nb-doped $(Bi_{0.5}Na_{0.4}K_{0.1})TiO_3$ lead-free ceramics, J. Mater. Sci. 52 (2017) 11337–11345.
[5] G. Dong, H. Fan, J. Shi, M. Li, Composition- and temperature-dependent large strain in (1-x)($0.8Bi_{0.5}Na_{0.5}TiO_3$-$0.2Bi_{0.5}K_{0.5}TiO_3$)-$x$$NaNbO_3$ ceramics, J. Am. Ceram. Soc. 98 (2015) 1150–1155.
[6] R. Kumari, N. Ahlawat, A. Agarwal, S. Sanghi, M. Sindhu, N. Ahlawat, Rietveld refinement, impedance spectroscopy and magnetic properties of $Bi_{0.8}Sr_{0.2}FeO_3$ substituted $Na_{0.5}Bi_{0.5}TiO_3$ ceramics, J. Magn. Magn Mater. 414 (2016) 1–9.
[7] Y.H. Kwon, G.H. Lee, J.H. Koh, Effects of sintering temperature on the piezoelectric properties of (Bi,Na)TiO_3-based composites for energy harvesting applications, Ceram. Int. 41 (2015) S792–S797.
[8] J.U. Rahman, A. Hussain, A. Maqbool, T.K. Song, W.J. Kim, S.S. Kim, M.H. Kim, Dielectric, ferroelectric and field-induced strain response of lead-free $BaZrO_3$-modified $Bi_{0.5}Na_{0.5}TiO_3$ ceramics, Curr. Appl. Phys. 14 (2014) 331–336.
[9] M. Liu, F. Lei, N. Jiang, Q. Zheng, D. Lin, Enhanced piezoelectricity, bright up-conversion and down-conversion photoluminescence in Er^{3+} doped $0.94(BiNa)_{0.5}TiO_3$-$0.06BaTiO_3$ multifunctional ceramics, Mater. Res. Bull. 74 (2016) 62–69.
[10] M. Zou, H. Fan, L. Chen, W. Yang, Microstructure and electrical properties of (1-x)[$0.82Bi_{0.5}Na_{0.5}TiO_3$-$0.18Bi_{0.5}K_{0.5}TiO_3$]-$x$$BiFeO_3$ lead-free piezoelectric ceramics, J. Alloys Compd. 495 (2010) 280–283.
[11] Q. Xu, M.T. Lanagan, W. Luo, L. Zhang, J. Xie, H. Hao, M. Cao, Z. Yao, H. Liu, Electrical properties and relaxation behavior of $Bi_{0.5}Na_{0.5}TiO_3$-$BaTiO_3$ ceramics modified with $NaNbO_3$, J. Eur. Ceram. Soc. 36 (2016) 2469–2477.
[12] A. Sasaki, T. Chiba, Y. Mamiya, E. Otsuki, Dielectric and piezoelectric properties of $(Bi_{0.5}Na_{0.5})TiO_3$-$(Bi_{0.5}K_{0.5})TiO_3$ systems, Jpn. J. Appl. Phys. 38 (1999) 5564–5567.
[13] K. Yoshii, Y. Hiruma, H. Nagata, T. Takenaka, Electrical properties and depolarization temperature of $(Bi_{1/2}Na_{1/2})TiO_3$-$(Bi_{1/2}K_{1/2})TiO_3$ lead-free piezoelectric ceramics, Jpn. J. Appl. Phys. 45 (2006) 4493–4496.
[14] R.A. Malik, A. Hussain, J.U. Rahman, A. Maqbool, T.K. Song, W.J. Kim, S.Y. Ryou, M.H. Kim, Structural transition and giant strain induced by A- and B-site concurrent donor doping in $Bi_{0.5}(Na_{0.84}K_{0.16})_{0.5}TiO_3$-$SrTiO_3$ ceramics, Mater. Lett. 143 (2015) 148–150.
[15] A. Khaliq, M. Sheeraz, A. Ullah, J.S. Lee, C.W. Ahn, I.W. Kim, Large strain in $Bi_{0.5}(Na_{0.78}K_{0.22})_{0.5}TiO_3$-$Bi(Mg_{0.5}Ti_{0.5})O_3$ based composite ceramics under low driving field, Sens. Act. A. 258 (2017) 174–181.
[16] A. Hussain, C.W. Ahn, A. Ullah, J.S. Lee, I.W. Kim, Dielectric, ferroelectric and field-induced strain behavior of $K_{0.5}Na_{0.5}NbO_3$-modified $Bi_{0.5}(Na_{0.78}K_{0.22})_{0.5}$-$TiO_3$ lead-free ceramics, Ceram. Int. 38 (2012) 4143–4149.
[17] Ar Ullah, R.A. Malik, A. Ullah, D.S. Lee, S.J. Jeong, J.S. Lee, I.W. Kim, C.W. Ahn, Electric-field-induced phase transition and large strain in lead-free Nb-doped BNKT-BST ceramics, J. Eur. Ceram. Soc. 34 (2014) 29–35.
[18] G.M. Osoro, D. Bregiroux, M.P. Thi, F. Levassort, Structural and piezoelectric properties evolution induced by cobalt doping and cobalt/niobium co-doping in $BaTiO_3$, Mater. Lett. 166 (2016) 259–262.
[19] Y. Yang, K. Liu, X. Liu, G. Liu, C. Xia, Z. He, Y. Yan, Electrical properties and microstructures of (Zn and Nb) co-doped $BaTiO_3$ ceramics prepared by microwave sintering, Ceram. Int. 42 (2016) 7877–7882.
[20] P. Ren, J. He, X. Wang, M. Sun, H. Zhang, G. Zhao, Colossal permittivity in niobium doped $BaTiO_3$ ceramics annealed in N_2, Scr. Mater 146 (2018) 110–114.
[21] Y.J. Kim, J.W. Hyun, H.S. Kim, J.H. Lee, M.Y. Yun, S.J. Noh, Y.H. Ahn, Microstructural characterization and dielectric properties of barium titanate solid solutions with donor dopants, Bull. Kor. Chem. Soc. 30 (2009) 1267–1273.
[22] B. Cui, P. Yu, J. Tian, H. Guo, Z. Chang, Preparation and characterization of niobium-doped barium titanate nanocrystalline powders and ceramics, Mater. Sci. Eng. A 454–455 (2007) 667–672.
[23] R.D. Shannon, Revised effective ionic radii and systematic studies of interatomic distances in halides and chalcogenides, Acta. Cryst A32 (1976) 751–767.
[24] P. Jaita, A. Watcharapasorn, D.P. Cann, S. Jiansirisomboon, Dielectric, ferroelectric and electric field-induced strain behavior of $Ba(Ti_{0.90}Sn_{0.10})O_3$-modified $Bi_{0.5}(Na_{0.80}K_{0.20})_{0.5}TiO_3$ lead-free piezoelectrics, J. Alloys Compd. 596 (2014) 98–106.
[25] T.H. Dinh, M.R. Bafandeh, J.K. Kang, C.H. Hong, W. Jo, J.S. Lee, Comparison of structural, ferroelectric, and strain properties between A-site donor and acceptor doped $Bi_{1/2}(Na_{0.82}K_{0.18})_{1/2}TiO_3$ ceramics, Ceram. Int. 41 (2015) S458–S463.
[26] N.B. Do, H.D. Jang, I. Hong, H.S. Han, D.T. Le, W.P. Tai, J.S. Lee, Low temperature sintering of lead-free $Bi_{0.5}(Na_{0.82}K_{0.18})_{0.5}TiO_3$ piezoelectric ceramics by co-doping with CuO and Nb_2O_5, Ceram. Int. 38S (2012) S359–S362.
[27] R.A. Malik, A. Hussain, A. Zaman, A. Maqbool, J.U. Rahman, T.K. Song, W.J. Kim, M.H. Kim, Structure-property relationship in lead-free A- and B-site co-doped $Bi_{0.5}(Na_{0.84}K_{0.16})_{0.5}TiO_3$-$SrTiO_3$ incipient piezoceramics, RSC Adv. 5 (2015) 96953–96964.
[28] B.D. Cullity, Elements of X-Ray Diffraction, second ed., Addison-Wesley, MA,

1978.
[29] B. Parija, S.K. Rout, L.S. Cavalcante, A.Z. Simões, S. Panigrahi, E. Longo, N.C. Batista, Structure, microstructure and dielectric properties of 100-x($Bi_{0.5}Na_{0.5}$)TiO_3-x[$SrTiO_3$] composites ceramics, Appl. Phys. A 109 (2012) 715–723.
[30] G. Liu, H. Fan, J. Shi, Z. Liu, Large strain and relaxation behavior in CeO_2 doped $Bi_{0.487}Na_{0.427}K_{0.06}Ba_{0.026}TiO_3$ piezoceramics, Ceram. Int. 42 (2016) 3938–3946.
[31] S. Bhandari, N. Sinha, B. Kumar, Enhanced microstructure and electrical properties of Mn-modified $Bi_{0.5}(Na_{0.65}K_{0.35})_{0.5}TiO_3$ ferroelectric ceramics, Ceram. Int. 42 (2016) 4274–4284.
[32] N. Pisitpipathsin, P. Kantha, K. Pengpat, M. Promsawut, S. Pojprapai, Effect of $KNbO_3$ on physical and electrical properties of lead-free $BaTiO_3$ ceramic, Ceram. Int. 41 (2015) 3639–3646.
[33] C. Kruea-In, T. Glansuvarn, S. Eitssayeam, K. Pengpat, G. Rujijanagul, Effects of NiO nanoparticles on electrical and magnetoelectric properties of BNT based ceramics, Electron. Mater. Lett. 9 (6) (2013) 833–836.
[34] P. Jaita, P. Butnoi, R. Sanjoom, C. Randorn, R. Yimnirun, G. Rujijanagul, Electric field-induced strain response of lead-free Fe_2O_3 nanoparticles modified $Bi_{0.5}(Na_{0.80}K_{0.20})_{0.5}TiO_3$-0.03($Ba_{0.70}Sr_{0.03}$)$TiO_3$ piezoelectric ceramics, Ceram. Int. 43 (2017) S2–S9.
[35] W. Bai, H. Li, J. Xi, J. Zhang, B. Shen, J. Zhai, Effect of different templates and texture on structure evolution and strain behavior of <001>-textured lead-free piezoelectric BNT-based ceramics, J. Alloys Compd. 656 (2016) 13–23.
[36] A. Hussain, A. Zaman, Y. Iqbal, M.H. Kim, Dielectric, ferroelectric and field induced strain properties of Nb-modified Pb-free 0.99$Bi_{0.5}(Na_{0.82}K_{0.18})_{0.5}TiO_3-0.01LiSbO_3$ ceramics, J. Alloys Compd. 574 (2013) 320–324.
[37] A. Hussain, J.U. Rahman, A. Zaman, R.A. Malik, J.S. Kim, T.K. Song, W.J. Kim, M.H. Kim, Field-induced strain and polarization response in lead-free $Bi_{1/2}(Na_{0.80}K_{0.20})_{1/2}TiO_3$-$SrZrO_3$ ceramics, Mater. Chem. Phys. 143 (2014) 1282–1288.
[38] E.M. Anton, W. Jo, D. Damjanovic, J. Rödel, Determination of depolarization temperature of ($Bi_{1/2}Na_{1/2}$)TiO_3-based lead-free piezoceramics, J. Appl. Phys. 110 (2011) 094108–094114.
[39] A. Ullah, A. Ullah, W.S. Woo, C.W. Ahn, I.W. Kim, Dielectric spectroscopy of lead-free $Bi_{0.5}(Na_{0.75}K_{0.25})_{0.5}TiO_3$-$BiAlO_3$ ceramics, Ceram. Int. 40 (2014) 11335–11342.
[40] C. Chalfouh, A. Lahmar, N. Abdelmoula, H. Khemakhem, Structural and dielectrics properties of Pr^{3+} doped $BaTi_{0.925}(Yb_{0.5}Nb_{0.5})_{0.075}O_3$ ceramics, J. Alloys Compd. 729 (2017) 858–865.
[41] X. Wei, Y. Feng, X. Wan, X. Yao, Evolvement of dielectric relaxation of barium stannate titanate ceramics, Ceram. Int. 30 (2004) 1397–1400.
[42] C. Kruea-In, S. Eitssayeam, K. Pengpat, T. Tunkasirit, G. Rujijanagul, Effect of vibro-milling on dielectric properties of barium zirconium titanate ceramics, Ferroelectrics 415 (2011) 135–140.
[43] N.V. Quyet, L.H. Bac, D. Odkhuu, D.D. Dung, Effect of Li_2CO_3 addition on the structural, optical, ferroelectric, and electric-field-induced strain of lead-free BNKT-based ceramics, J. Phys. Chem. Solid. 85 (2015) 148–154.
[44] H. Gao, X. Hao, Q. Zhang, S. An, L.B. Kong, Thickness-dependent electrocaloric effect of $Pb_{0.82}Ba_{0.08}La_{0.10}(Zr_{0.90}Ti_{0.10})O_3$ antiferroelectric thick films, J. Alloys. Compd. 690 (2017) 131–138.
[45] N. Vittayakorn, G. Rujijanagul, X. Tan, M.A. Marquardt, D.P. Cann, The morphotropic phase boundary and dielectric properties of the $x$$PbZr_{1/2}Ti_{1/2}O_3$-(1-$x$)$PbNi_{1/3}Nb_{2/3}O_3$ perovskite solid solution, J. Appl. Phys. 96 (2004) 5103–5109.
[46] G. Ray, N. Sinha, B. Kumar, Environment friendly novel piezoelectric 0.94[$Na_{0.8}K_{0.2}NbO_3$]-0.06$LiNbO_3$ ternary ceramic for high temperature dielectric and ferroelectric applications, Mater. Chem. Phys. 142 (2013) 619–625.
[47] Q. Zheng, J. Ma, D. Lin, Microstructure, dielectric and piezoelectric properties of La-modified $Bi_{0.5}(Na_{0.84}K_{0.16})_{0.5}TiO_3$ lead-free ceramics, J. Mater. Sci. Mater. Electron. 24 (2013) 3836–3843.
[48] F. Wang, M. Xu, Y. Tang, T. Wang, W. Shi, C.M. Leung, Large strain response in the ternary $Bi_{0.5}Na_{0.5}TiO_3$-$BaTiO_3$-$SrTiO_3$ solid solutions, J. Am. Ceram. Soc. 95 (2012) 1955–1959.
[49] K. Wang, A. Hussain, W. Jo, J. Rödel, Temperature-dependent properties of ($Bi_{1/2}Na_{1/2}$)TiO_3-($Bi_{1/2}K_{1/2}$)TiO_3-$SrTiO_3$ lead-free piezoceramics, J. Am. Ceram. Soc. 95 (2012) 2241–2247.
[50] J. Hao, X. Zhang, Z. Xu, R. Chu, W. Li, P. Fu, J. Du, Field-induced large strain in lead-free 0.99[(1-x)$Bi_{0.5}(Na_{0.80}K_{0.20})_{0.5}TiO_3$-$x$$BiFeO_3$]-0.01($K_{0.5}Na_{0.5}$)$NbO_3$ piezoelectric ceramics, Ceram. Int. 42 (2016) 12964–12970.
[51] L. Ramajo, J. Camargo, F. Rubio-Marcos, M. Castro, Influences of secondary phases on ferroelectric properties of Bi(Na,K)TiO_3 ceramics, Ceram. Int. 41 (2015) 5380–5386.
[52] S.T. Zhang, B. Yang, W. Cao, The temperature-dependent electrical properties of $Bi_{0.5}Na_{0.5}TiO_3$-$BaTiO_3$-$Bi_{0.5}K_{0.5}TiO_3$ near the morphotropic phase boundary, Acta Mater. 60 (2012) 469–475.
[53] M. Chandrasekhar, Sonia, P. Kumar, Synthesis and characterizations of $NaNbO_3$ modified BNT-BT-BKT ceramics for energy storage applications, Physica B 497 (2016) 59–66.
[54] Y. Zhao, J. Xu, L. Yang, C. Zhou, X. Lu, C. Yuan, Q. Li, G. Chen, H. Wang, High energy storage property and breakdown strength of $Bi_{0.5}(Na_{0.82}K_{0.18})_{0.5}TiO_3$ ceramics modified by $(Al_{0.5}Nb_{0.5})^{4+}$ complexion, J. Alloys Compd. 666 (2016) 209–216.
[55] Y. Zhao, J. Xu, C. Zhou, C. Yuan, Q. Li, G. Chen, H. Wang, L. Yang, High energy storage properties and dielectric behavior of $(Bi_{0.5}Na_{0.5})_{0.94}Ba_{0.06}Ti_{1-x}(Al_{0.5}Nb_{0.5})_xO_3$ lead-free ferroelectric ceramics, Ceram. Int. 42 (2016) 2221–2226.
[56] R.A. Malik, A. Hussain, A. Maqbool, A. Zaman, T.K. Song, W.J. Kim, M.H. Kim, Giant strain, thermally-stable high energy storage properties and structural evolution of Bi-based lead-free piezoelectrics, J. Alloys Compd. 682 (2016) 302–310.
[57] L. Zhang, X. Hao, L. Zhang, Enhanced energy-storage performances of Bi_2O_3-Li_2O added (1-x)($Na_{0.5}Bi_{0.5}$) TiO_3-$x$$BaTiO_3$ thick films, Ceram. Int. 40 (2014) 8847–8851.
[58] R.A. Malik, A. Hussain, A. Maqbool, A. Zaman, C.W. Ahn, J.U. Rahman, T.K. Song, W.J. Kim, M.H. Kim, Temperature-insensitive high strain in lead-free $Bi_{0.5}(Na_{0.84}K_{0.16})_{0.5}TiO_3-0.04SrTiO_3$ ceramics for actuator applications, J. Am. Ceram. Soc. 98 (2015) 3842–3848.
[59] K.T. Lee, J.S. Park, J.H. Cho, Y.H. Jeong, J.H. Paik, J.S. Yun, Phase transition and electrical characteristic of $Bi_{0.5}(Na_{0.78}K_{0.22})_{0.5}TiO_3$-$BiFeO_3$ lead-free piezoelectric ceramics, Ceram. Int. 41 (2015) 10298–10303.
[60] S.T. Zhang, A.B. Kounga, E. Aulbach, T. Granzow, W. Jo, H.J. Kleebe, J. Rödel, Lead-free piezoceramics with giant strain in the system $Bi_{0.5}Na_{0.5}TiO_3$-$BaTiO_3$-$K_{0.5}Na_{0.5}NbO_3$. I. structure and room temperature properties, J. Appl. Phys. 103 (2008) 034107.
[61] X.Y. Tong, H.L. Li, J.J. Zhou, H. Liu, J.Z. Fang, Giant electrostrain under low driving field in $Bi_{1/2}Na_{1/2}TiO_3$-$SrTiO_3$ ceramics for actuator applications, Ceram. Int. 42 (2016) 16153–16159.
[62] M. Saleem, M.S. Kim, I.S. Kim, S.J. Jeong, Polarization and strain behaviors of 0.74$BiNaTiO_3$-0.26$SrTiO_3$/$Bi_{0.5}(Na_{0.8}K_{0.2})_{0.5}TiO_3$ ceramic composite, Ceram. Int. 42 (2016) 13960–13968.
[63] S.T. Zhang, F. Yan, B. Yang, W. Cao, Phase diagram and electrostrictive properties of $Bi_{0.5}Na_{0.5}TiO_3$-$BaTiO_3$-$K_{0.5}Na_{0.5}NbO_3$ ceramics, Appl. Phys. Lett. 97 (2010), 122901.
[64] K.T.P. Seifert, W. Jo, J. Rödel, Temperature insensitive large strain of ($Bi_{1/2}Na_{1/2}$)TiO_3-($Bi_{1/2}K_{1/2}$)TiO_3-($K_{0.5}Na_{0.5}$)NbO_3 lead-free piezoceramics, J. Am. Ceram. Soc. 93 (2010) 1392–1396.
[65] V.D.N. Tran, T.H. Dinh, H.S. Han, W. Jo, J.S. Lee, Lead-free $Bi_{1/2}(Na_{0.82}K_{0.18})_{1/2}TiO_3$ relaxor ferroelectrics with temperature insensitive electrostrictive coefficient, Ceram. Int. 39 (2013) S119–S124.